Multi-layer thin-film electrolytes for metal supported solid oxide fuel cells

M. Haydn[a,*], K. Ortner[b], T. Franco[a], S. Uhlenbruck[c], N.H. Menzler[c], D. Stöver[c], G. Bräuer[b],
A. Venskutonis[a], L.S. Sigl[a], H.P. Buchkremer[c], and R. Vaßen[c]

[a] Plansee SE, A-6600 Reutte, Austria
[b] Fraunhofer Institute for Surface Engineering and Thin Films, D-38108 Braunschweig, Germany
[c] Forschungszentrum Jülich, 52428-Jülich, Germany

* corresponding author
Tel.: +43-5672-600-2007
E-mail address: markus.haydn@plansee.com

Abstract

A key to the development of metal supported solid oxide fuel cells (MSCs) is the manufacturing of gas-tight thin-film electrolytes, which separate the cathode from the anode. In this paper the electrolytes are applied by a physical vapor deposition (PVD) gas flow sputtering (GFS) process. The gas-tightness of the electrolyte is significantly improved when sequential oxide and metallic thin-film multi-layers, which interrupt the columnar grain structure of single-layer electrolytes, are deposited. Such electrolytes with 8 oxide/metal layers and a total thickness of about 4 µm obtain leakage rates of less than 3.10^{-4} hPa dm^3 s^{-1} cm^{-2} (Δp: 100 hPa, 22.3 cm^2 measurement area) at room temperature. They are also highly tolerant with respect to surface flaws and particulate impurities which can be present on the gradient anode underground. Preliminary tests with a two-level stack of MSCs, still with a single-layer electrolyte, feature a power density of 420 mW cm^{-2} at 800°C and underline the high potential of MSC cells.

Keywords: SOFC, Fuel Cell, MSC, ITM

1 Introduction

In the last decades, global development and industrializing activities in the field of solid oxide fuel cells (SOFCs) were dominated by two cell technologies, i.e. the anode-supported (ASC) and the electrolyte-supported (ESC) cell. Both cell types have demonstrated highly efficient power generation and cost effective cell manufacturing by using well established ceramic processing technologies such as screen printing and tape casting. Supported by the high development efforts, SOFC systems are currently giving their debut in commercial markets, e.g. in stationary power and/or combined heat and power (CHP) applications [1, 2].

Besides stationary applications, the interest for mobile and portable power generation has been growing continuously during the past years. SOFC system requirements for such applications being very challenging, e.g. frequent redox- and thermo-cycles as well as short start-up times, it was readily realized that ceramic ASC and ESC cell technologies do not suffice the demands. To meet this challenge, developments to create SOFCs based on a metal-supported cell (MSC) technology were initiated [3-5]. Reinforced by a metallic support, an MSC combines significantly improved mechanical stability with a much enhanced thermal and redox behavior as compared to fully ceramic cell systems, and thus addresses all important requirements for mobile applications.

Plansee’s activities in the field of component development for the MSC date back to the 1990s. At that time, a ferrite oxide dispersion strengthened Fe-Cr-alloy (trade name ITM) was developed which is processed in a powder-metallurgical (P/M) manufacturing route. Key milestones of the development are shown in Fig. 1.1.

Fig. 1.1. Milestones of Plansee’s MSC component development

From 2001 till 2003, the development was focused on gastight interconnects and other high-temperature components as well as ITM foils and thin stamped metal sheets [6]. Porous metallic ITM substrates and initial protective coatings – comprising doped $LaCrO_3$ and $LaMnO_3$ – were developed from 2003 until 2008, e.g. for diffusion barrier layers at the substrate-anode interface and to reduce the Cr-evaporation at the interconnector’s cathode side. Those tasks were predominantly performed using the plasma-spray MSC concept of DLR Stuttgart and described in detail elsewhere [7-9].

Based on a close collaboration with Forschungszentrum Jülich (Jülich) and Karlsruhe Institute of Technology (KIT), Plansee has been developing active MSC components since 2008, i.e. ITM supported anode-electrolyte-cathode assemblies, which are targeted to meet the requirements of a high performance thin-film MSC [10, 11]. Only recently, based on screen printing and thin-film PVD technologies, Plansee has set up an industrial pilot line to meet market demands for high performance metal-supported cells and “ready-to-stack” repeat units, e.g. for auxiliary power units (APUs) in diesel-powered heavy trucks [12].

Plansee’s generic cell development program was supported by the “NextGen MSC” project in cooperation with Jülich, KIT and AVL List GmbH respectively, and funded by the German Ministry of Economics and Technology (BMWi). Whereas Jülich and KIT were providing a high level of basic scientific support to the cell development, Plansee and AVL engaged in the industrial commercialization, including a pilot manufacturing line for MSC cells and repeat-units, and system-relevant testing of MSC stacks for the truck APU in a prototype environment.

In the follow-up project, “MetAPU”, which is also being financially supported by BMWi, and will be running until mid of 2014, a first generation of a metal-supported cell will be integrated in a light-weight design for a truck APU. The MSC design was developed in close collaboration with ElringKlinger AG, while the scientific support and the system relevant stack-testing within this project were supplied by Jülich.

The work presented in this paper is focused on the development of thin-film electrolytes for the current cell design. It was performed within the NextGen MSC-project jointly between Plansee and the Fraunhofer Institute for Surface Engineering and Thin Films (Fraunhofer IST). In this work “gas flow sputtering”, a powerful physical vapor deposition (PVD) process was used to develop and integrate gas-tight and thin (< 5 µm) electrolyte structures for high-performance MSCs.

2 Experimental

2.1 Powder metallurgical manufactured porous substrate

The porous metallic substrate is the backbone of the MSC and must fulfill the following requirements:

i) It must be highly porous to ensure sufficient gas transport to the anode. The porosity must be stable under long-term operation in reducing atmospheres at temperatures up to 850 °C.
ii) It must be highly creep resistant to ensure long-term structural integrity.
iii) The coefficient of thermal expansion (CTE) of the metallic substrate must match the CTE of the ceramic cell layers as closely as possible.
iv) The electrical conductivity of the substrate must be preserved under long-term operation even at the cathode side where oxide scales can reduce the conductivity significantly.
v) Cr evaporation on cathode side poisons the cathode and must be suppressed.

All requirements are fulfilled by the oxide dispersion strengthened (ODS) alloy ITM (Fe26Cr (Mo, Ti), Y_2O_3)) [13, 14]. An SEM micrograph of the cross section of ITM and a 3D topography scan of its surface are shown in Fig. 2.1.

Fig. 2.1. SEM cross-section of the ITM-substrate (left), 3-dimensional optical surface scan of the ITM-substrate (x: y: z=1: 1: 1, $\Delta z=0{,}089$ mm) (right) [15]

The porosity of the ITM substrate is homogenously distributed over the whole cross section as well as at the surface. Notably, a sufficient fuel gas (H_2, CO …) distribution and supply to the MSC anode as well as the removal of the exhaust gases (H_2O, CO_2) must be ensured. The subsequent cell layers, particularly the graded anode, can be smoothly deposited as consequence of the flatness of the ITM surface.

2.2 Structure and manufacturing route of metal supported solid oxide fuel cells

The primary structure of the MSC is a porous ITM-substrate with a thickness of ≈ 1 mm. On top of this backbone, thin-film cell layers are deposited by different procedures. A schematic cross-section of an MSC is shown in Fig. 2.2.

Fig. 2.2. Schematic cross-section scheme of a metal supported cell [15]

The manufacturing route of the MSC is as follows:

i) First, a 1-2 µm gadolinium doped ceria (GDC) layer is placed onto the ITM-substrate via magnetron sputtering. This GDC constitutes a diffusion barrier layer (DBL) which prevents (i) the diffusion of Ni from the anode into the ITM-substrate and (ii) the diffusion of Fe and Cr from the substrate into the anode [16].
ii) Subsequently, an anode with a total thickness of 40-70 µm, which features a distinct pore- and grain-size gradient, is applied by screen printing and successive sintering. While the porosity of the starting layer on top of the GDC is coarse, the pore and grain size of the subsequent anode layers decrease gradually such that a very smooth and flat surface is achieved at the top anode layer. Sufficient smoothness and planarity of the anode surface are prerequisites to deposit an electrolyte layer which is both thin and gas-tight. SEM cross-sections of the substrate-anode assembly and scans of the anode surface are shown in Fig. 2.3.
iii) Then, the electrolyte with a thickness 4-5 µm is applied by a physical vapor deposition gas flow sputtering (GFS) process.
iv) On top of the electrolyte a second 1-2 µm thick GDC protective layer is deposited by magnetron sputtering. The function of this layer is to prevent the formation of electrically isolating Strontium-Zirconium-phases between the electrolyte and the cathode [17-19].
v) Finally, a 20-60 µm porous LSCF ($La_{1-x}Sr_xFe_{1-y}Co_yO_{3-\delta}$) cathode layer is screen printed. The activation and sintering of the cathode occurs during the start-up of cell operation.

Fig. 2.3. SEM cross-section of the ITM-substrate with graded anode (top) and 3-dimensional optical surface scans of the anode with x: y: z=1: 1: 1; scan area 1 mm x 1 mm with Δz=0,02 mm (bottom left) scan area 0,05 mm x 0,05 mm with Δz=0,004 mm (bottom right).

2.3 Production of thin-film electrolytes by a gas-flow sputtering process

At the Fraunhofer Institute for Surface Engineering and Thin Films (Fraunhofer IST) a unique physical vapor deposition (PVD) process, called “gas-flow sputtering” (GFS), has been developed during the past years. GFS has many advantages as compared to conventional PVD-sources. Among others there are (i) high deposition rates up to 10 µm h^{-1} and (ii) high process pressures of about 0.5 mbar [20-22], which both foster fast and economic processing. Furthermore, the source design is well adapted for reactive operation conditions such that oxides, carbides and nitrides can be deposited [22].

2.3.1 The gas-flow-sputtering source

Fig. 2.4 shows the cross-section scheme of a GFS-source. The metallic targets (1) are water-cooled (2) and connected to the cathode potential of a source generator (3). The process gas Argon is fed in at position (4) and flows through the source. At the end of the source, reactive gases (5) can be fed in to grow oxides, nitrides or carbides. The substrate (6) is mounted on the substrate holder (7), which can be moved in front of the source to increase the deposition area. It can be necessary to heat the substrate, e.g. with ceramic heaters (8). To increase the density of deposited layers, the substrate holder can be negatively biased with a pulsed-DC (direct current) generator (9). If sufficient power is supplied and the process pressure is in the right range, the hollow cathode plasma burns between the metallic targets. Target atoms are released from the target by sputtering and transported along with the argon stream onto the substrate.

Fig. 2.4. Cross-section scheme of a GFS-source [20, 21].

2.3.2 Setup of the Gas-flow-Sputtering facility

Fig. 2.5 shows the set-up of a gas flow sputtering system. The octagonal recipient (1) has a volume of about 200 liters and 4 door flanges. The pumping speed (2) is ≈ 1000 $m^3 h^{-1}$, the chamber pressure is recorded by a capacitance manometer (MKS Baratron® (3)). The linear GFS-sputter source (4) has a length of 250 mm and is flange-mounted horizontally on a door-flange. The pretreatment facility (5) is flange-mounted on a door-flange too. A metallic zirconium-yttrium-alloy (85.2 at.-% Zr, 14.8 at.-% Y) is used as target material to deposit 8YSZ (8 mol.-% Y_2O_3 stabilized ZrO_2) in the reactive mode. A pulsed-DC generator (6) is applied as source generator (Pinnacle Plus, Advanced Energy) which supplies the source in DC-modus. The process and reactive gas supply is guaranteed by a gas flow regulation system (MKS, Multi-Gas Controller 647B (7)). The substrate movement is realized by a turntable (8) onto which the substrate holder is mounted (9). A multiphase motor enables the positioning and the oscillation movement during the coating process. A medium frequency bias-voltage is applied on the substrate holders via a MF-Plasma-Generator (ENI, RPG-50, 5 kW Puls-DC) (10). This medium frequency bias-voltage enables the coating of non-conducting layers as e.g. oxides. The substrate is heated by ceramic heaters which are fed by a Xantrex XRF 300-9 power supply (11) and the temperature is measured on the substrate holder directly by thermocouples (12).

Fig. 2.5. Gas-flow-sputtering system at Fraunhofer IST in Braunschweig, Germany

2.3.3 Process control and typical coating parameters of thin film GFS-electrolytes

First the substrate is fixed on the substrate holder, then the recipient is evacuated and the substrate is heated. Next the substrate is pretreated by putting a bias-voltage on the substrate holder until a glow discharge arises, which activates the substrate surface (table 2.1). Subsequently, the GFS-source is turned on and the substrate holder commutes in front of the source to enable the coating of large areas. During the first seconds of electrolyte processing, the reactive gas feeding is disabled to deposit a very thin metallic adherent layer between the anode and the electrolyte which is thought to improve adhesion. Table 2.1 summarizes typical pretreatment and process parameters of GFS-electrolyte coatings.

Tab. 2.1. Typical electrolyte coating parameters

Process parameter	**Pretreatment**	**Coating**
Inert gas (Argon) in sccm	300-500	4000-6000
Reactive gas (O_2) in sccm	0	50-100*
Process-pressure in 10^{-6} bar	≈ 100	≈ 500
Source-power in W	0	4000-6000
Bias-voltage in V	≥ 100	50-150
Duration of process step in min	10	≈ 15-30
Substrate-temperature in °C	≈ 500	≈ 500

∗ the reactive gas is switched on after 10 s (metallic adherent layer)

The pressure is adjusted by an Argon gas flow which enables a hollow cathode glow discharge. With reactive (O_2) gas flow rates of 50-100 sccm, O^{2-} conductive 8YSZ layers can be deposited from the metallic Zirconium-Yttrium-targets. Based on typical coating parameters shown in table 2.1, three different electrolyte configurations were developed:

i) Single-layer electrolyte:
It is applied in reactive mode with 50-100 sccm O_2, such that a continuous 8YSZ electrolyte with a typical thickness of 3-5 µm is generated.

ii) Double layer electrolyte:
The first layer (3-5 µm) of the electrolyte is sputtered in reactive mode (50-100 sccm O_2) and subsequently a thin top layer (300-500 nm) is deposited in metallic mode (no O_2). Unexpectedly, the discontinuity between the oxide base-layer and the metallic top-layer promoted the gas-tightness of the entire electrolyte. However, since the metallic layer cannot conduct O^{2-}-ions, the electrolyte must be heat-treated in an oxygen-containing atmosphere to finally transform the metallic film into 8YSZ. That transformation occurs during the start-up of cell operation.

iii) Multi-layer electrolyte:
The electrolyte consists of a sequence of 8 thin layers (300-500 nm) which are sputtered alternately in metallic (no O_2) and reactive (50-100 sccm O_2) mode. The resulting electrolyte structure further improves the gas-tightness of the assembly, especially less addicted to the underground structure. Again, the metallic layers are transformed into 8YSZ during the start-up of cell operation.

A key quality criterion of an MSC is its electrolyte performance. Firstly, the electrolyte must safely separate the anode from the cathode side to ensure high open cell voltages (OCV). Secondly, reduction of internal impedance demands electrolytes to be as thin as possible to ensure high power densities.

To compare the gas-tightness of electrolytes, the leakage-rates were carefully assessed. The measurement set-up is as follows: vacuum is applied on a sealed electrolyte surface area and the pressure increase is recorded. In this paper the leakage-rate is reported in hPa $dm^3s^{-1}cm^{-2}$ at a pressure difference of 100 hPa.

2.5 Electrochemical characterization methods

Initial electrochemical characterizations of state of the art single-layer MSCs (see Fig. 3.3) were performed at Jülich in a two level stack which was joined by sealing glass. LSCF was used as cathode material and the active cell-layers is ≈ 84 cm^2 per level. After a start-up phase of approx. 100 hours, 2 Nl/min H_2 with a humidity of 10 % and 2 Nl/min Argon were fed to the anode and 10 Nl/min air was fed to the cathode side.

3 Results

3.1 Anode impact on the GFS-electrolyte

As discussed in chapter 2.2, the anode and the cathode of the MSC are separated by a thin-film 8YSZ electrolyte. Firstly a graded structure is deposited onto the ITM-substrate to reduce the pore-size at the anode surface. This is the prerequisite to allow an effective sealing of the porous anode by a gas-tight thin-film GFS-electrolyte. Initially, six different graded anodes with various porosity and particle size distributions were developed and the growth behavior of the GFS thin-film electrolyte was examined in reactive deposition mode (50-100 sccm O_2, single-layer electrolyte). To compare the six anodes, they were coated at the same time in the same process using the process parameters from table 2.1. Fig. 3.1 shows the SEM images of two anode variants with as-deposited electrolytes.

Fig. 3.1. SEM cross-sections: fracture surfaces (left) and polished cross-section with marked pores (right) of two anode structures which were electrolyte-coated simultaneously. Coarse anode structure (AV3) (top), fine anode structure (AV6) (bottom).

The left side of Fig. 3.1 displays SEM micrographs of fracture surfaces and on the right side the corresponding polished cross sections are shown. The microstructures of the two anodes differ strongly, i.e. the anode AV3 (top) features coarse particles and pores and is generally less homogeneous than the anode AV6 (bottom). Obviously, the morphology of the GFS-electrolytes re-echo their corresponding anode surface topography, demonstrating that the latter structure decides largely on the performance of the coating. It will be shown later that the coating sequence is another decisive processing element, which nevertheless builds decisively on a well prepared anode surface.

One major goal in MSC-development is to manufacture cells with an electrolyte as thin as possible. Notably, a thickness of 4-5 µm is far too thin to create gas-tight electrolytes on the coarse AV3 anode structure (Fig. 3.1 top), whereas the gas tightness of the fine anode structure AV6 (Fig. 3.1 bottom) is acceptable at that thickness level.

Fig. 3.2. Leakage rates of four electrolyte coating processes (various bias-voltages) on six anode variants (AV1 – AV6)

Fig. 3.2 compares the leakage rates of 4 electrolyte modifications (different bias-voltages) which were deposited onto six different anode variants. Again, all anode variants were processed simultaneously. Notably, the anode structure impacts the gas permeability significantly more than the bias-voltage. The leakage rate of anode AV6 in Fig. 3.1 (bottom) is, depending slightly on the bias-voltage, almost two orders of magnitude lower than of the AV3 anode in Fig. 3.1 (top). Hence, a fine-grained, homogenous and flat anode surface leads to electrolytes which safely separate the anode from the cathode gases.

Fine-tuning of the electrolyte microstructure becomes feasible through the bias voltage. Based on the results for AV6, a 4 µm electrolyte (reactive mode; 50-100 sccm O_2, adapted bias-voltage), MSCs suitable for electrochemical characterization can be produced. Fig. 3.3 shows a cross-section of an optimized MSC half-cell (without cathode), which already contains a thin-film GDC diffusion barrier layer. With the optimized MSCs in Fig. 3.3 leakage rates of 2.10^{-4} hPa dm^3 s^{-1} cm^{-2} (Δp: 100 hPa, 22.3 cm^2 measurement area, room temperature) were obtained. From a geometric point of view it appears feasible to seal the AV6 anode structure with an even thinner electrolyte. However, experiments have demonstrated that the AV6 anode requires at least a 4 µm single-layer electrolyte to obtain sufficient gas tightness.

Fig. 3.3. State of the art MSC (type: MSC06b) without cathode layer

3.2 Flaws in the electrolyte

Beside the dominant impact of the anode structure on the gas-tightness of the electrolyte, coating defects as well as impurities of the anode surface finally control the integrity of the electrolyte. Fig. 3.4 depicts representative coating flaws in thin-film electrolytes. The spallation in Fig. 3.4a results from high residual compression in the electrolyte layer. Driven by these stresses, the electrolyte buckles with the fracture origin being either a delamination at the anode-electrolyte interface or a crack in the anode structure.

Fig. 3.4. Typical electrolyte coating defects; bulges and spallation (a), nodular growth (b), accretion growth (c), outburst (d). Note the different magnifications of (a) and (b-d)

Gas-tight electrolytes can be manufactured by using high bias-voltages on the one hand and thick electrolytes on the other hand. Both parameters stress the substrate and at a certain point the typical failures shown in Fig. 3.4 occur [23]. Therefore a compromise between electrolyte thickness, bias-voltage and leakage rate is mandatory to manufacture large-area, defect-free MSCs.

As already pointed out in chapter 3.1, the integrity of the electrolyte depends mainly on the surface structure of the graded anode. If, moreover, particulate impurities are also present at the anode surface, nodular defects can develop [24-26]. Examples for such flaws are shown in Fig. 3.4b, c. The nodules are more or less strongly bonded to the surrounding electrolyte and will be typically pulled above a certain layer thickness threshold. In that case cavities are left behind the pulled-out nodule as illustrated in Fig. 3.4d. Evidently, embedded flaws increase the leakage rate less than cavities, because the latter weaken the electrolyte morphology geometrically thereby increasing the leakage rate.

Accordingly, a dust free environment is mandatory during manufacturing of the anode to avoid nodular defects as effectively as possible. As discussed in chapter 2.2, the anode is applied by multi-layer screen printing followed by a sintering process. To this end, the screen printing paste must be very homogeneous to avoid local inhomogeneity at the anode surface which would disturb the integrity of gas-tight electrolytes or raise the required electrolyte thickness. The influence of the anode structure on the required electrolyte thickness and the influence of surface impurities were examined by a numerical simulation and will be discussed in a forthcoming paper.

3.3 Electrolyte structures

As shown above, it is the pore size distribution and the flatness of the anode surface which control the microstructure and the integrity of the growing electrolyte. Nevertheless, if flaws and particulate impurities are present at the anode surface, they are reproduced in the electrolyte structure and may generate flaws as well. To reduce these impacts, the layered electrolyte structures can be deposited either by

(i) sputtering of a separate 300-500 nm metallic film (no O_2 addition) on top of the initial oxide layer (50-100 sccm O_2) or
(ii) applying a series of alternating 300-500 nm metallic (no O_2 addition) and reactive oxide (50-100 sccm O_2) thin films.

Fig. 3.5. Different electrolytes comprising reactive and metallic layers [metallic layers (m), oxide electrolyte layers (o)]; 4 µm pure oxide electrolyte (top); 3.5 µm oxide layer with 0.5 µm metallic top layer (center); electrolyte compound of four 0.5 µm metallic and four 0.5 µm oxide layers (bottom);

Fig. 3.5 displays SEM images of three horizontally layered electrolyte configurations. The electrolyte in the top SEM image of Fig. 3.5 contains a 4 µm single oxide layer (2. 10^{-4} hPa dm^{3}s^{-1}cm^{-2}), the electrolyte in the center comprises a two-layer electrolyte with a 3.5 µm oxide and a 0.5 µm metallic film (8. 10^{-4} hPa dm^{3}s^{-1}cm^{-2}), and finally the multi-layer electrolyte in the bottom of Fig. 3.5 is made up of eight alternating 0.5 µm metallic and 0.5 µm oxide films (3. 10^{-4} hPa dm^{3}s^{-1}cm^{-2}). The leakage rates were measured at Δp 100 hPa, a measurement area of 22.3 cm^2 and room temperature. Obviously, switching from the metallic to the reactive deposition mode (or vice versa), triggers a change in the electrolyte's morphology.

Firstly it should be noted that, as the crystallite growth is interrupted after each layer, the grain size of that layer is confined to the particular layer thickness. Consequently, the columnar 8YSZ crystals in a single layer electrolyte extend from the anode to the cathode interface. The recurring layer structure however, breaks up the columnar structure, as new crystals grow in each layer. This morphology suppresses the development of potential flaws along the columnar grains of pure oxide electrolytes and, consequently, improves the gas tightness of the electrolyte. Thus, by introducing layered electrolytes it is feasible to seal porous anode structures more effectively.

3.4 Electrochemical characterization of a two-level MSC Stack

The electrical characteristics of a two-level stack (single-layer MSC) are presented in Fig. 3.6 which plots the cell voltages of both levels as a function of stack operation time. Based on problems with the test rig wiring of cell 1 the potential drops at the very beginning of the test. Yet after having that problem fixed, both cells behave similarly with an open cell voltage of about 1 V. Beyond the start-up phase, the voltages achieve more than 1 V for both cells. The fairly high cell potentials indicate low leakage rates of the electrolytes at operation temperature.

Fig. 3.6. Electrochemical characterization of a two-level MSC Stack (Fuel gas: 2 Nl/min H_2, 2 Nl/min Ar, 10% H_2O; Oxide gas: 10 Nl/min Air)

After the start-up phase, the U-I-characteristics of both cell levels were measured at different operation temperatures (700 °C, 750 °C and 800 °C). The characteristic curves are shown in the bottom diagram of Fig. 3.6. At higher operation temperatures the cells supply higher current densities, and again both cells perform equally well. At 800°C and 0.7 V the stack yields a power-density of about 420 mW cm^{-2}. Due to the progressive aging of cell 2, the stack was switched off after 381 hours of operation. Follow-up examinations showed that the aging effect was primarily caused by problems with the sealing glass. However, the electrochemical characterization demonstrates the fundamental functionality and the high potential of the developed thin-film MSCs.

4 Conclusions

Starting from a porous P/M Fe-Cr-substrate (ITM), a metal supported cell was developed successfully. The key feature of this MSC is a gas-tight and well adherent thin-film electrolyte which was deposited by gas flow sputtering (GFS). To achieve sufficiently low leakage rates, an electrolyte thickness > 4 µm is required. Analysis of SEM-images reveal, that defects and particulate impurities of and at the anode surface raise the required electrolyte width and explain why the actually observed 4 µm film thickness threshold is needed. Depositing electrolyte structures with alternating reactive oxide and metallic layers, significantly improves the impermeability of the electrolytes significantly and, simultaneously, reduces the effects of anode surface flaws and particles.

Finally, a two-level prototype stack was manufactured and tested successfully. It was demonstrated that the new single-layer MSCs have the potential to perform well in technical stacks. Specifically, a power density of 420 mW cm^{-2} (@ 0.7 V, 800 °C operation temperature, 2 x 84 cm^2 active cell area, 10 % humidity on anode side) was achieved. This indicates the substantial potential of this MSC-type for mobile applications, e.g. for the electrical power supply in SOFC truck auxiliary power units.

5 Acknowledgements

The authors would like to acknowledge Prof. Ludger Blum (Jülich) and Dipl.-Ing. Ute Packbier (Jülich) for the electrochemical characterization of the 2-level MSC stack.

6 References

[1] www.bloomenergy.com

[2] R. Payne, J. Love, and Michael Kah, “CFCL’s BlueGen Product, “Proc. Solid Oxide Fuel Cell, Montreal, pp. 81-85, (2011), S. Singhal, K. Eguchi, SOFC-XII

[3] N. Christiansen, H. Holm-Larsen, S. Primdahl, M. Wandel, S. Ramousse, A. Hagen: Recent Progress in Development and Manufacturing of SOFC at Topsoe Fuel Cell A/S and Risø DTU. ECS Transactions, 35 (2011). Proceedings of the SOFC-XII Symposium at the 219th ECS Meeting, Montreal, Canada, 1 to 6 May 2011

[4] G. Schiller, T. Franco, R. Henne, M. Lang, R. Ruckdäschel, P. Otschik , K. Eichler: Proc. SOFC-VII, Electrochem. Soc. Vol. 2001 Iss. 16 (2001), 885-894

[5] Th. Franco, R. Mücke, M. Rüttinger, N. Menzler, L.G.J. de Haart, and Andreas Venskutonis, in Proceedings of 9th European Solid Oxide Fuel Cell Forum, P. Connor, Editor, 16-20, Lucerne, Switzerland (2010)

[6] W. Glatz, G. Kunschert, A. Venskutonis, SOFC-IX, Vol. 2, S.C. Singhal, J. Mizusake (eds.), ECS Proceedings Volume 2005-07, 1773-1780 (2005)

[7] Th. Franco, R. Henne, “Metallic Components for a Plasma Sprayed Thin-Film SOFC Concept”, in Solid Oxide Fuel Cells VIII (SOFC-VIII), Hrsg.: S.C. Singhal und M. Dokiya, Electrochemical Society, Pennington, NJ, (2003), pp. 923-932

[8] G. Kunschert, K. H. Kailer, S. Schlichtherle, and G. N. Strauss, “Ceramic PVD Coatings as Dense/Thin Barrier Layers on Interconnect Components for SOFC Applications”, Proceedings of 8th European SOFC Forum, Lucerne/Switzerland, July 2008

[9] Th. Franco, K. Schibinger, Z. Ilhan, G. Schiller, and A. Venskutonis, “Ceramic Diffusion Barrier Layers for Metal Supported SOFCs”, in Solid Oxide Fuel Cells X (SOFC-X)-Part 1, Ed. K. Eguchi, S.C. Singhal, H. Yokokawa, J. Mitzusaki, Vol. 7, no. 1, (2007), pp. 771-780, ISBN 978-1-56677-555-7.

[10] Th. Franco, R. Mücke, M. Rüttinger, N. Menzler, L.G.J. de Haart, and Andreas Venskutonis, in Proceedings of 9th European Solid Oxide Fuel Cell Forum, P. Connor, Editor, 16-20, Lucerne, Switzerland (2010).

[11] M. Rüttinger, R. Mücke, Th. Franco, O. Büchler, N. H. Menzler, and A. Venskutonis, „Metal-Supported Cells with Comparable Performance to Anode-Supported Cells in Short-Term Stack Environment", Proc. Solid Oxide Fuel Cell, Montreal, pp. 259-269, (2011), S. Singhal, K. Eguchi, SOFC-XII.

[12] J. Rechberger and P. Prenninger, SAE Technical Paper Series 2007-01-4273, World Congress, Detroit, (2007).

[13] A.Venskutonis, G. Kunschert, M. Brandner, Th. Franco, F. Jansen; Recent Progress in Powdermetallurgical "Ready to Stack " Interconnect Components for various SOFC Applications; A0906; Abstract 220; Oral Presentation; Interconnects and Coatings; 2008

[14] B. Tabernig, Th. Franco, A. Venskutonis, H. Kestler, L. S. Sigl; Properties of a P/M FeCr Alloy as Interconnect Material for Solid Oxide Fuel Cells; Proceedings, EURO PM 2011, Barcelona, Spain, 2011

[15] M. Haydn, Th. Franco, R. Mücke, M. Rüttinger, N. H. Menzler, A. Weber, A. Venskutonis, L.S. Sigl; A Novel Manufacturing Route for Metal Supported Thin-Film Solid Oxide Fuel Cells; PM-2012; Yokohama; Japan

[16] M. C. Tucker; Progress in metal-supported solid oxide fuel cells: A review; Journal of Power Sources 195 (2010) 4570-4582

[17] H. Yokokawa, N. Sakai, T. Horita, K. Yamaji, M. E. Brito, H. Kishimoto; Thermodynamic and kinetic considerations on degradations in solid oxide fuel cell cathodes; Journal of Alloys and Compounds 452 (2008) 41-47

[18] S. Uhlenbruck, N. Jordan, D. Sebold, H. P. Buchkremer, V. A. C. Haanappel, D. Stöver; Thin film coating technologies of (Ce,Gd)O2 – _ interlayers for application in ceramic high-temperature fuel cells; Thin Solid Films 515 (2007) 4053-4060

[19] H. Yokokawa, H. Tu, B. Iwanschitz, A. Mai; Fundamental mechanisms limiting solid oxide fuel cell durability; Journal of Power Sources 182 (2008) 400-412

[20] S. Tang, U. Schulz; Gas flow sputtering - An approach to coat complex geometries and Non Line of Sight areas; Surface & Coatings Technology 204 (2009) 1087-1091

[21] K. Ortner, M. Birkholz, Th. Jung; Neue Entwicklungen beim Hohlkathoden- Gasflusssputtern; Vakuum in Forschung und Praxis 15 (2003) Nr. 5 236-239

[22] Th. Jung, T. Kälber, V. v.d. Heide; Gas flow sputtering of oxide coatings: practical aspects of the process; Surface and Coatings Technology 86-87 (1996) 218-224

[23] R. W. Knoll, E. R. Bradley; Correlation between the stress and microstructure in Bias-Sputtered ZrO2-Y2O3 films; Thin Solid Films, 117 (1984) 201-210

[24] X. Liu, D. Li, Y. Zhao, X. Li; Further investigations of the characteristics of nodular defects; Applied Optics, Vol. 49, No. 10, April 2010

[25] K. H. Guenther; Nodular defects in dielectric multilayers and thick single layers; Applied Optics, Vol. 20, No. 6, March 1981

[26] R. Mattheis, F. Thrum, H.-J. Anklam; Nodular growth in thin films: Preparation and transmission electon microscopy characterization in CoCr layers on silicon substrates; Thin Solid Films, 188 (1990) 335-340

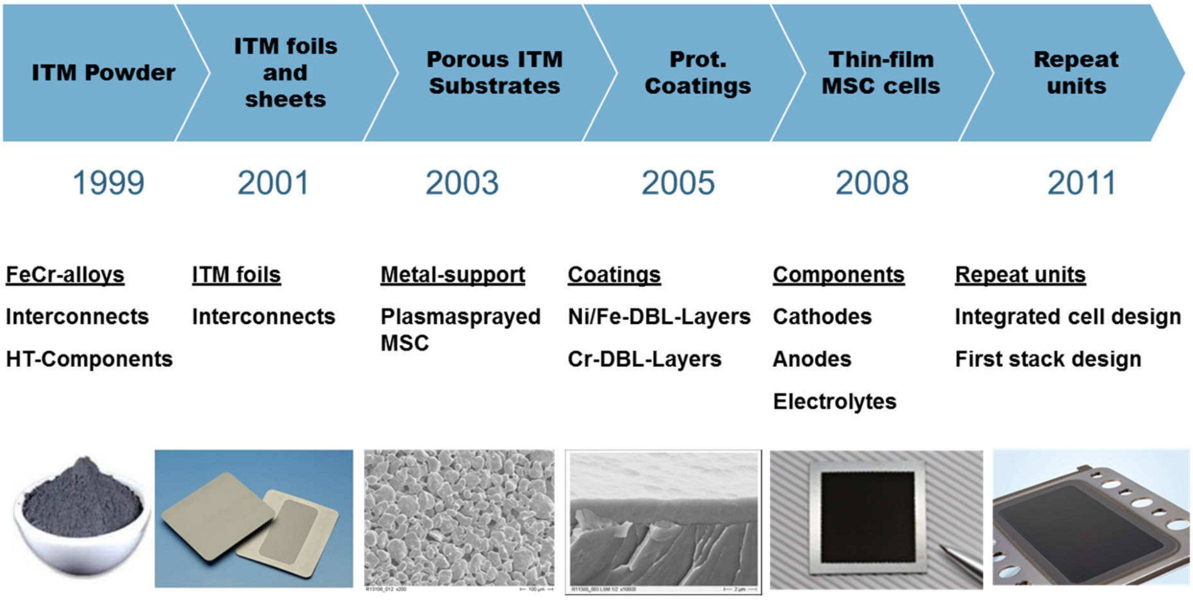

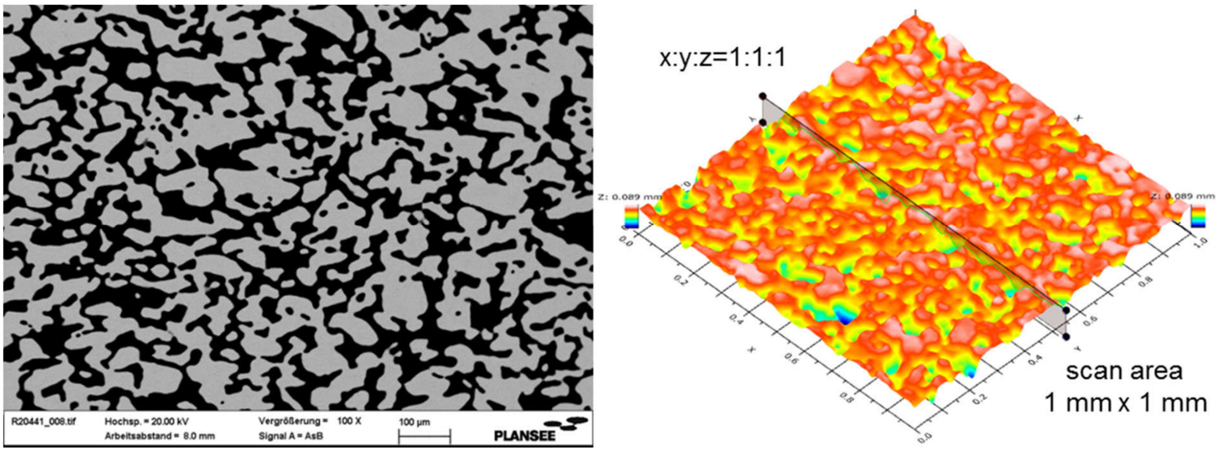
R20441_008.tif
Hochsp. = 20.00 kV
Arbeitsabstand = 8.0 mm
Vergrößerung = 100 X
Signal A = AsB
100 µm
PLANSEE
x:y:z=1:1:1
Z: 0.089 mm
Z: 0.089 mm
0.0
0.2
0.4
0.6
0.8
1.0
X
Y
scan area
1 mm x 1 mm

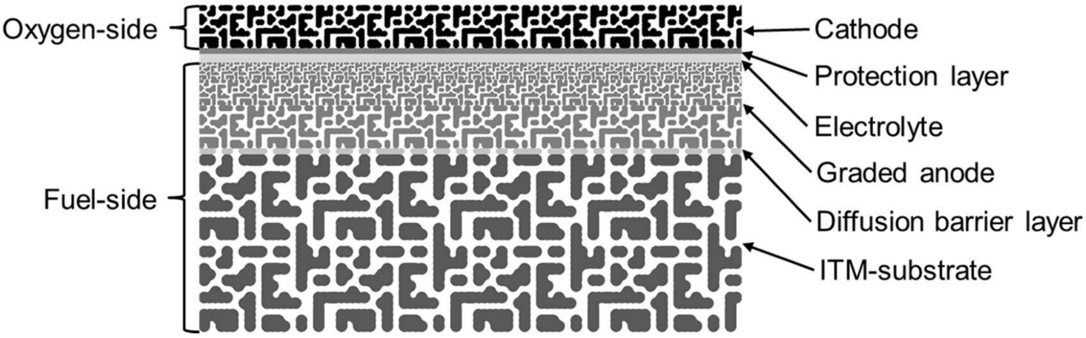
Oxygen-side
Fuel-side
Cathode
Protection layer
Electrolyte
Graded anode
Diffusion barrier layer
ITM-substrate

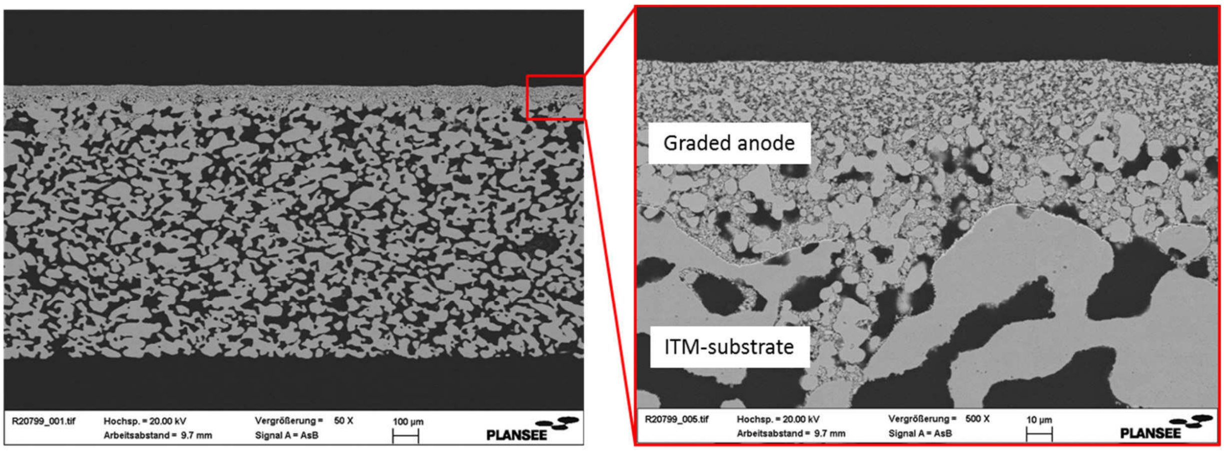
Graded anode
ITM-substrate
R20799_001.tif
Hochsp. = 20.00 kV
Arbeitsabstand = 9.7 mm
Vergrößerung = 50 X
Signal A = AsB
100 µm
PLANSEE
R20799_005.tif
Hochsp. = 20.00 kV
Arbeitsabstand = 9.7 mm
Vergrößerung = 500 X
Signal A = AsB
10 µm
PLANSEE

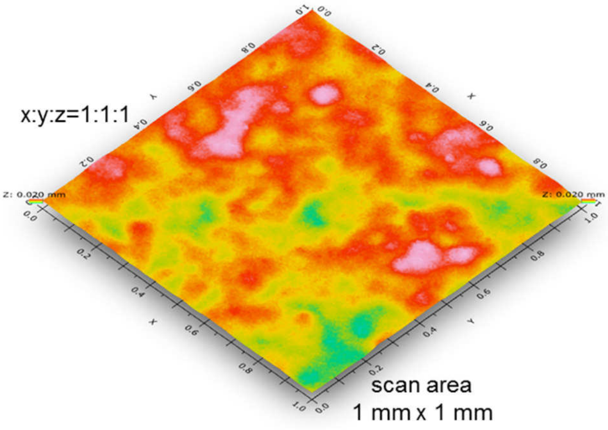
x:y:z=1:1:1
Z: 0.020 mm
scan area
1 mm x 1 mm

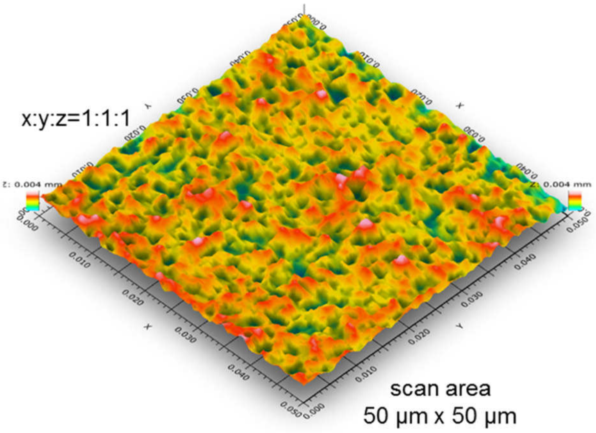
x:y:z=1:1:1
Z: 0.004 mm
scan area
50 µm x 50 µm

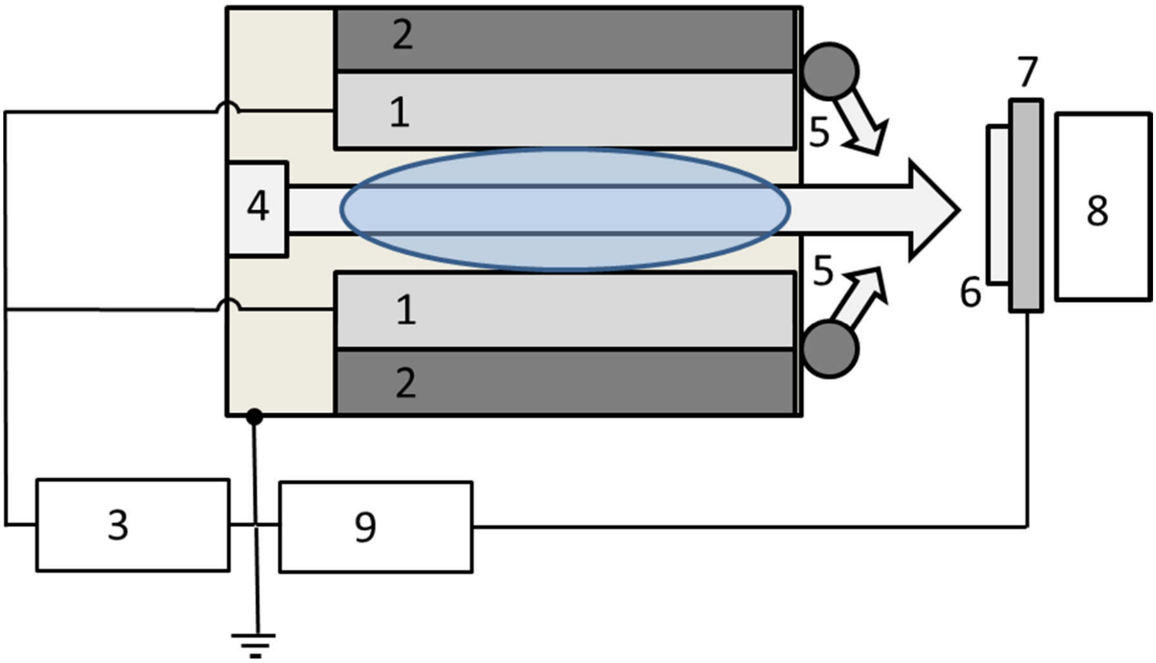
2
1
5
4
5
1
2
7
6
8
3
9

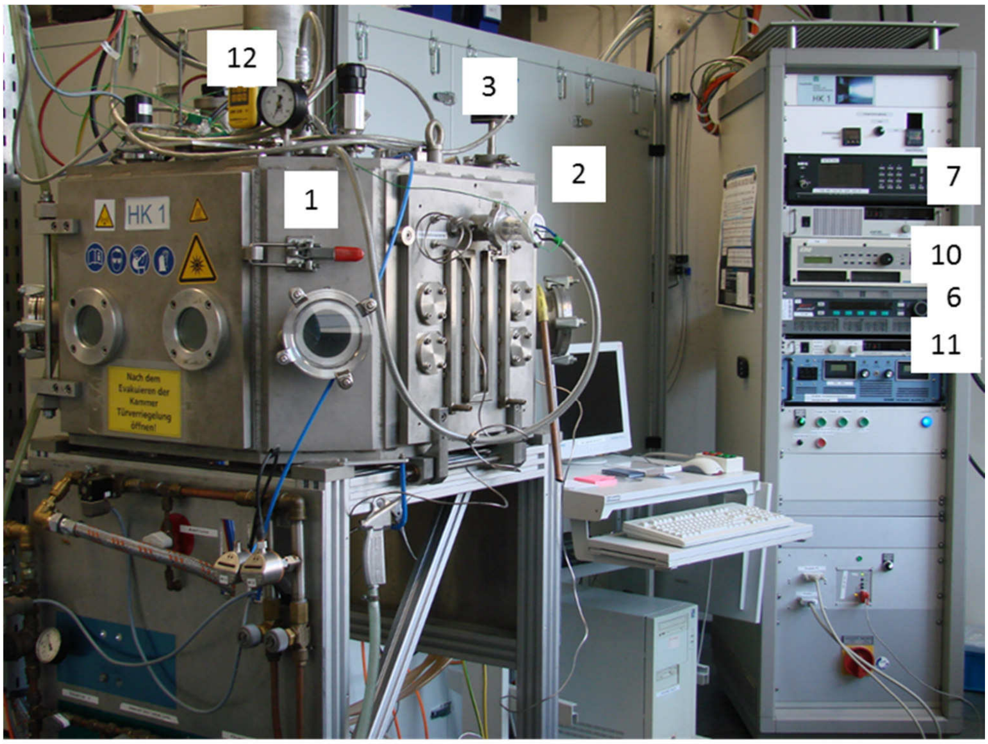
12
3
1
2
HK 1
Nach dem Evakuieren der Kammer Türverriegelung öffnen!
7
10
6
11

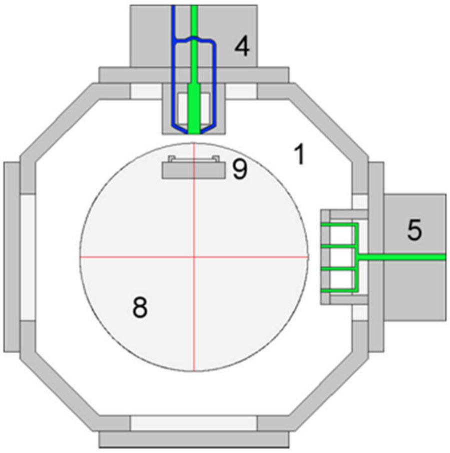
4
1
9
5
8

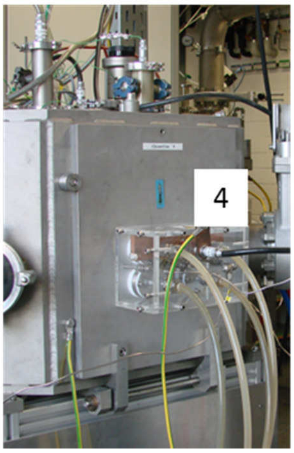
4

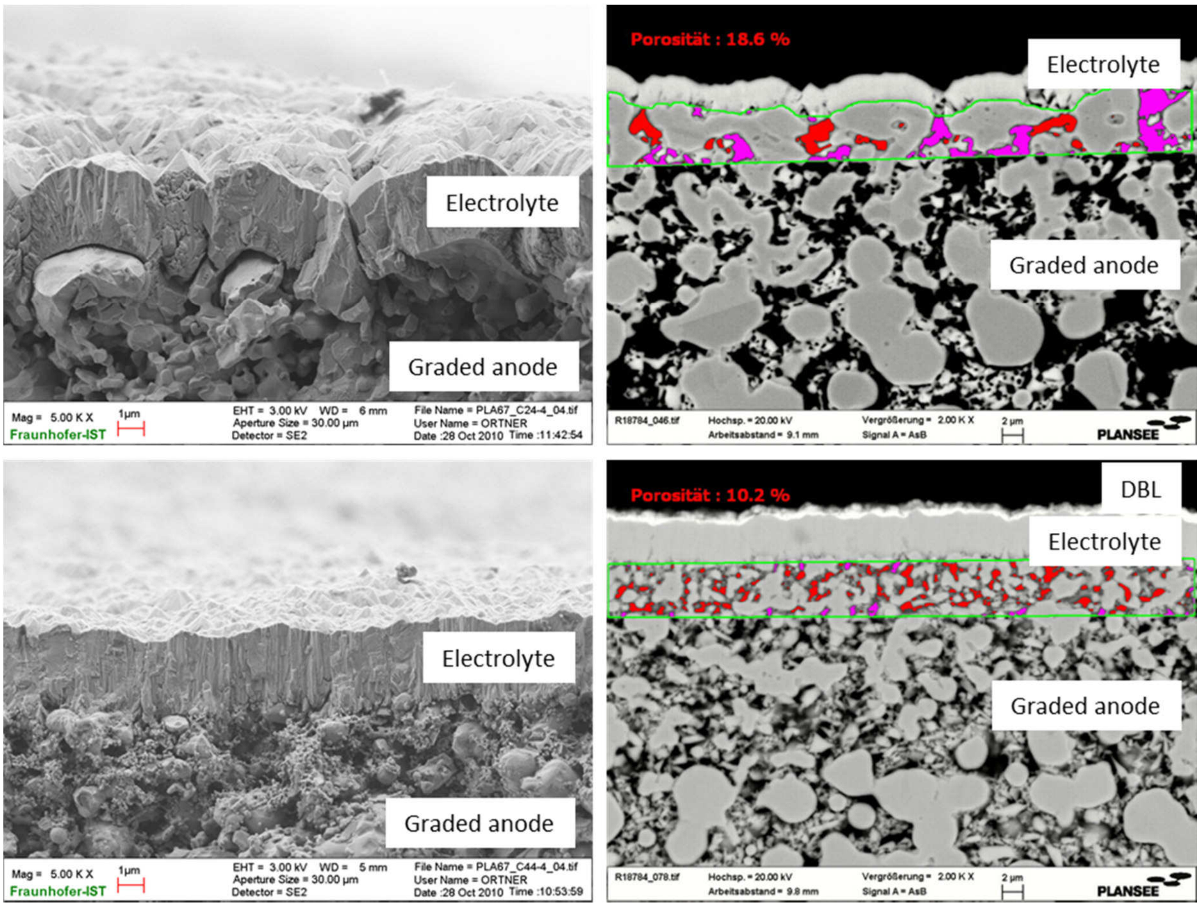
Electrolyte
Graded anode
Mag = 5.00 K X
1µm
Fraunhofer-IST
EHT = 3.00 kV WD = 6 mm
Aperture Size = 30.00 µm
Detector = SE2
File Name = PLA67_C24-4_04.tif
User Name = ORTNER
Date :28 Oct 2010 Time :11:42:54
Porosität : 18.6 %
Electrolyte
Graded anode
R18784_046.tif
Hochsp. = 20.00 kV
Arbeitsabstand = 9.1 mm
Vergrößerung = 2.00 K X
Signal A = AsB
2 µm
PLANSEE
Electrolyte
Graded anode
Mag = 5.00 K X
1µm
Fraunhofer-IST
EHT = 3.00 kV WD = 5 mm
Aperture Size = 30.00 µm
Detector = SE2
File Name = PLA67_C44-4_04.tif
User Name = ORTNER
Date :28 Oct 2010 Time :10:53:59
Porosität : 10.2 %
DBL
Electrolyte
Graded anode
R18784_078.tif
Hochsp. = 20.00 kV
Arbeitsabstand = 9.8 mm
Vergrößerung = 2.00 K X
Signal A = AsB
2 µm
PLANSEE

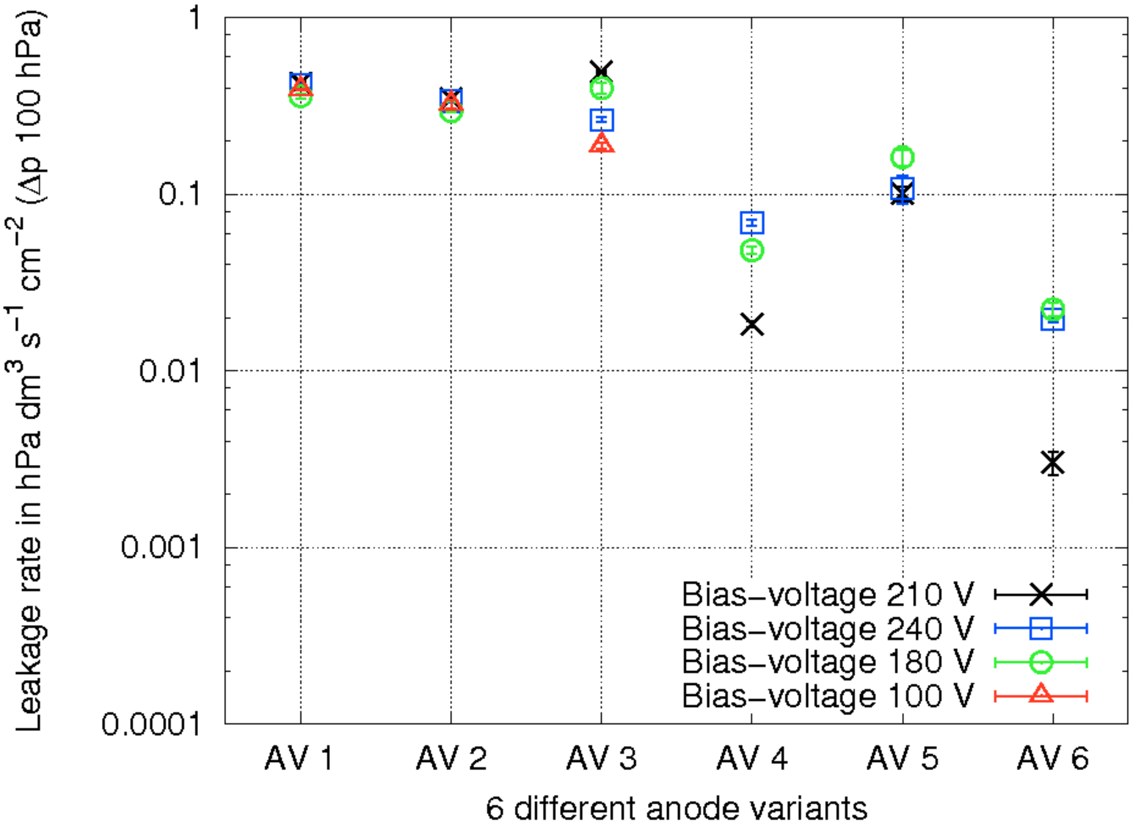
Leakage rate in hPa dm^3 s^{-1} cm^{-2} (Δp 100 hPa)
1
0.1
0.01
0.001
0.0001
AV 1
AV 2
AV 3
AV 4
AV 5
AV 6
6 different anode variants
Bias–voltage 210 V
Bias–voltage 240 V
Bias–voltage 180 V
Bias–voltage 100 V

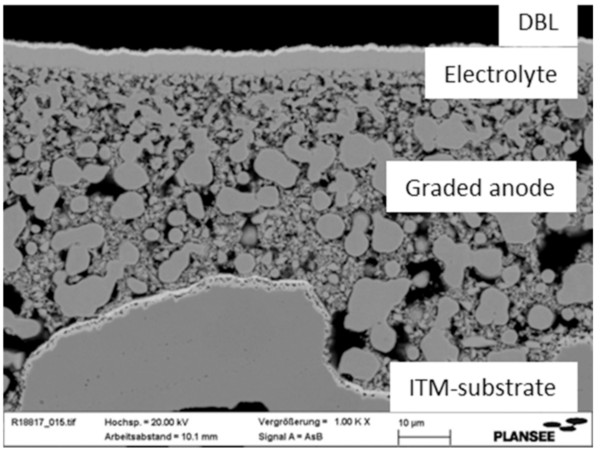
DBL
Electrolyte
Graded anode
ITM-substrate
R18817_015.tif
Hochsp. = 20.00 kV
Arbeitsabstand = 10.1 mm
Vergrößerung = 1.00 K X
Signal A = AsB
10 µm
PLANSEE

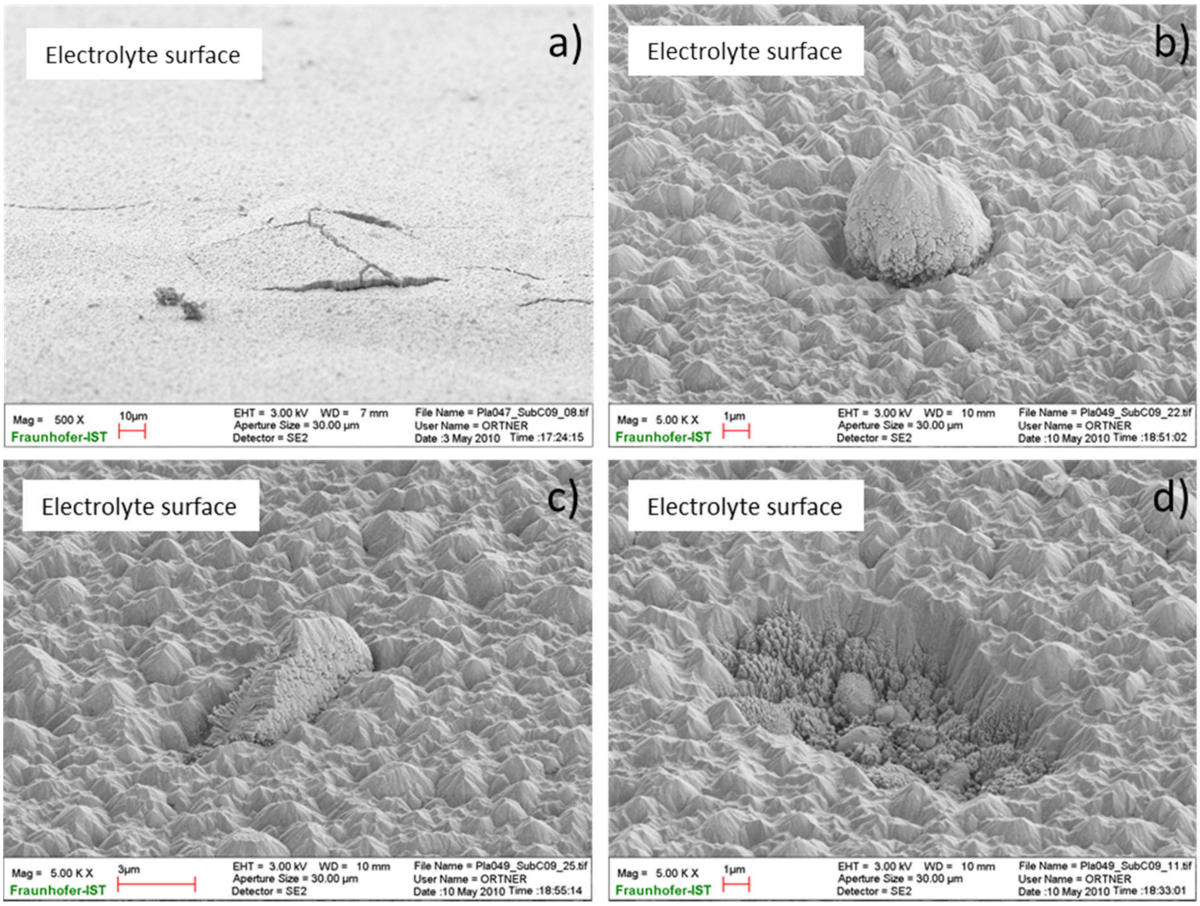
Electrolyte surface
a)
Mag = 500 X
10µm
Fraunhofer-IST
EHT = 3.00 kV WD = 7 mm
Aperture Size = 30.00 µm
Detector = SE2
File Name = Pla047_SubC09_08.tif
User Name = ORTNER
Date :3 May 2010 Time :17:24:15
Electrolyte surface
b)
Mag = 5.00 K X
1µm
Fraunhofer-IST
EHT = 3.00 kV WD = 10 mm
Aperture Size = 30.00 µm
Detector = SE2
File Name = Pla049_SubC09_22.tif
User Name = ORTNER
Date :10 May 2010 Time :18:51:02
Electrolyte surface
c)
Mag = 5.00 K X
3µm
Fraunhofer-IST
EHT = 3.00 kV WD = 10 mm
Aperture Size = 30.00 µm
Detector = SE2
File Name = Pla049_SubC09_25.tif
User Name = ORTNER
Date :10 May 2010 Time :18:55:14
Electrolyte surface
d)
Mag = 5.00 K X
1µm
Fraunhofer-IST
EHT = 3.00 kV WD = 10 mm
Aperture Size = 30.00 µm
Detector = SE2
File Name = Pla049_SubC09_11.tif
User Name = ORTNER
Date :10 May 2010 Time :18:33:01

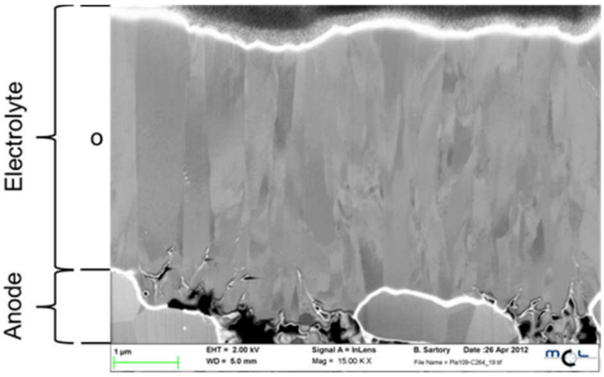
Electrolyte
o
Anode
1 µm
EHT = 2.00 kV
WD = 5.0 mm
Signal A = InLens
Mag = 15.00 K X
B. Sartory
Date :26 Apr 2012
File Name = Pla109-C264_19.tif
mcl

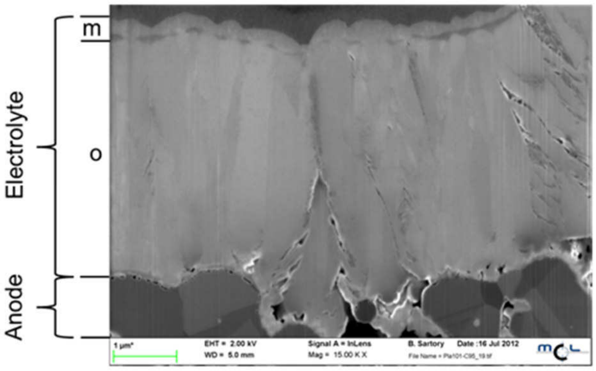
m
Electrolyte
o
Anode
1 µm*
EHT = 2.00 kV
WD = 5.0 mm
Signal A = InLens
Mag = 15.00 K X
B. Sartory
Date :16 Jul 2012
File Name = Pla101-C95_19.tif
mcl

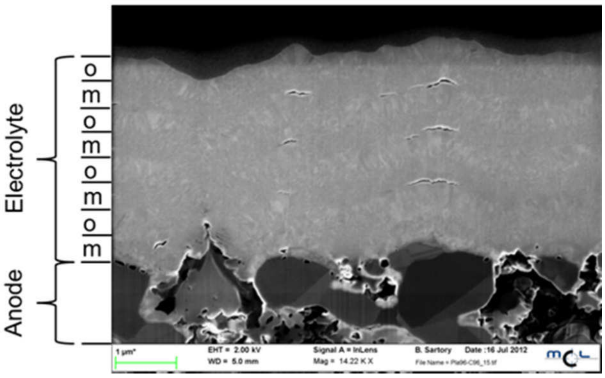
o
m
o
m
o
m
o
m
Electrolyte
Anode
1 µm*
EHT = 2.00 kV
WD = 5.0 mm
Signal A = InLens
Mag = 14.22 K X
B. Sartory
Date :16 Jul 2012
File Name = Pla96-C96_15.tif
mcl

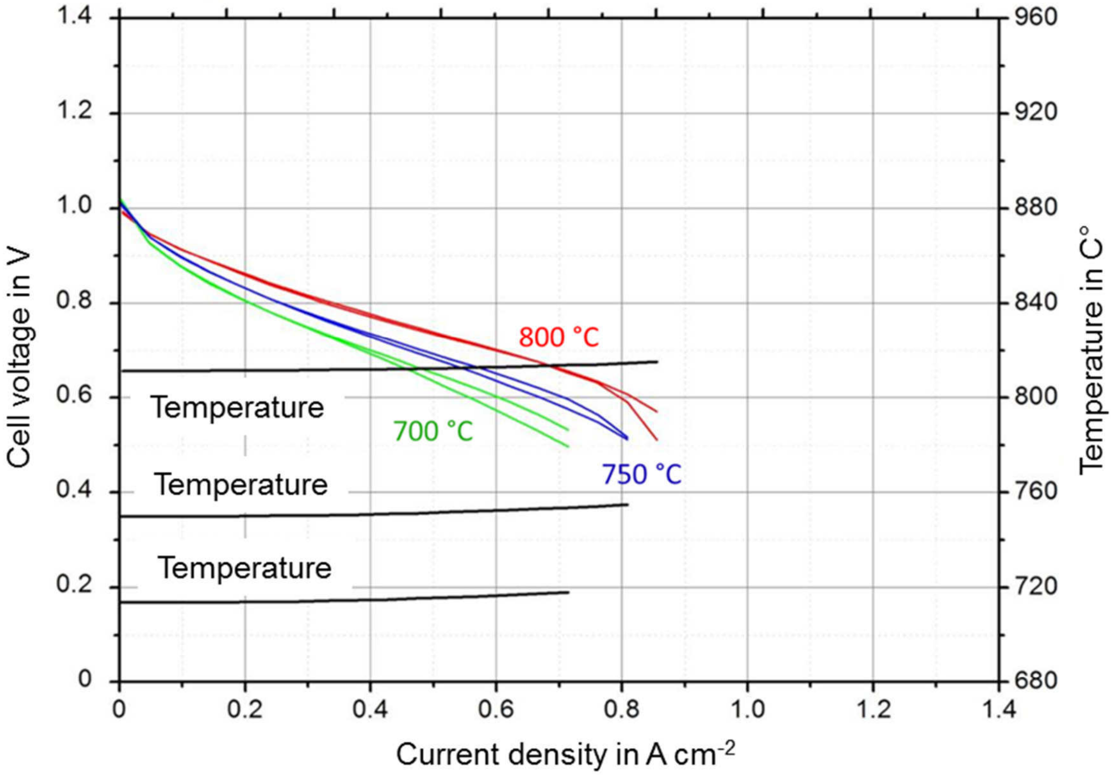
Cell voltage in V
1.4
1.2
1.0
0.8
0.6
0.4
0.2
0
Temperature in C°
960
920
880
840
800
760
720
680
Current density in A cm^{-2}
0
0.2
0.4
0.6
0.8
1.0
1.2
1.4
800 °C
700 °C
750 °C
Temperature
Temperature
Temperature

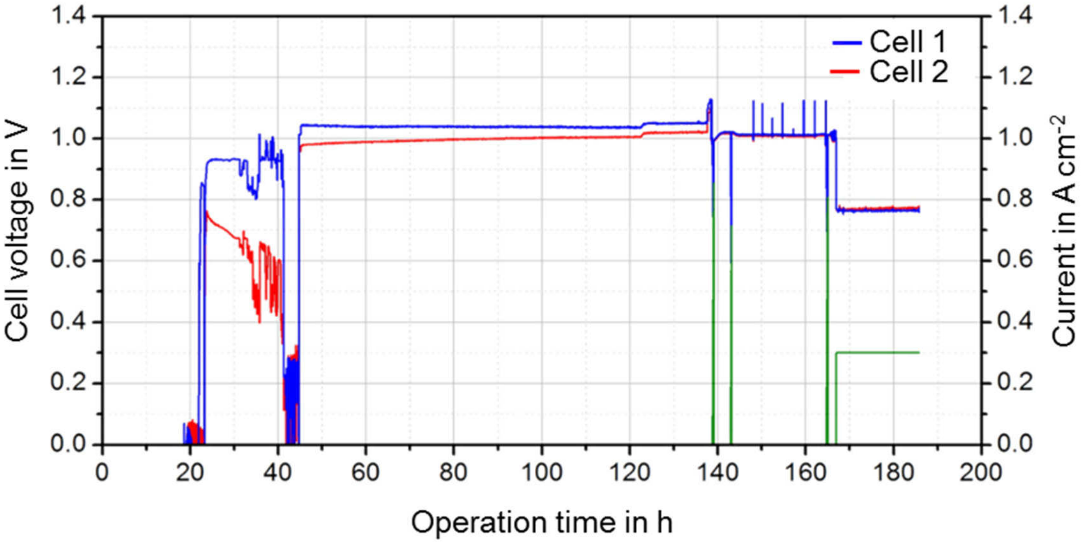
Cell 1
Cell 2
Cell voltage in V
1.4
1.2
1.0
0.8
0.6
0.4
0.2
0.0
Current in A cm^{-2}
1.4
1.2
1.0
0.8
0.6
0.4
0.2
0.0
Operation time in h
0
20
40
60
80
100
120
140
160
180
200